AIAA'83

AIAA-83-1752

Supercritical Cascade Flow Analysis with Shock-Boundary Layer Interaction

P. Niederdrenk,
H. Sobieczky, DFVLR-AVA, Göttingen, FRG;
D. S. Dulikravich, Univ. of Texas, Austin, TX

AIAA 16th Fluid and Plasma Dynamics Conference

July 12-14, 1983/ Danvers, Massachusetts

SUPERCRITICAL CASCADE FLOW ANALYSIS WITH SHOCK-BOUNDARY LAYER INTERACTION

Peter Niederdrenk* and Helmut Sobieczky*
DFVLR, Göttingen, F.R. Germany

George S. Dulikravich**
University of Texas at Austin

Abstract

The paper describes improvements made to a user oriented analysis code for steady twodimensional transonic flows in turbomachinery cascades. The full potential equation is solved by a finite area technique, using a C-type grid and an analytical wake model. Solution adaptive grid clustering refines the inviscid shock representation. The boundary layer is computed by an integral method except in the shock region, where the analytical interaction model of Bohning and Zierep smoothes out the pressure distribution on the airfoil surface. The code is applied in its analysis and design modes to an experimentally tested cascade.

Nomenclature

a	speed of sound
c	cascade airfoil maximum chord length
C_p	pressure coefficient
g	gap distance between leading edges of two neighbouring airfoils in the cascade
$H_{32} = \delta_3/\delta_2$	boundary layer shpae factor
M	Mach number
Re	Reynolds number
	velocity components in physical plane (x,y)
U,V	contravariant velocity vector components in computational plane (X,Y)
α	free stream angle
β	cascade stagger angle
δ_1	displacement thickness
δ_2	momentum thickness
δ_3	energy thickness
ϕ	velocity potential
ρ	fluid density
ξ,η	artificial viscosity components
ω	relaxation coefficient

Introduction

Analysis of compressor flow is often based on an interactive use of approximate models for two gross features of the flow: the throughflow, which is approximated as an axisymmetric flow between hub and tip contours, and the blade-to-blade flow, which is treated as nearly twodimensional in planes tangent to the axisymmetric streamfunction surfaces. In this paper we confine ourselves to the latter part, the transonic cascade flow.

At high subsonic inlet Mach numbers transonic cascade flow is usually characterized by local supersonic regions on the blades' suction sides. In order to avoid strong shock losses and minimize viscous losses the blades should be shaped to provide supercritical flow with nearly isentropic recompression at the design point. The general aim is to obtain larger operating ranges over inlet Mach number and incidence while keeping the losses acceptably low at the same time. During off-design performance these losses are mainly due to normal shock waves terminating the supersonic bubble and interacting with the boundary layer. Small changes in the profile's thickness in the order of the boundary layer displacement thickness, particularly in the supersonic region, may shift a shockless cascade flow into a shocked flow.

Thus, careful blade design requires an accurate prediction method including viscous/inviscid interaction effects. Though solving the Navier-Stokes equations in the whole flow field would certainly be the most complete model, in view of the simplifying assumptions already introduced we prefer the much faster approach of iterating solutions in different parts of the flowfield to a composite solution until convergence is achieved. At the high Reynolds numbers of practical interest the shear layers are thin and viscous effects can be attributed to an overall viscous/inviscid interaction between boundary layer, wake and external inviscid flow. The generally weak global interaction may be significantly augmented at transonic speeds by strong local interactions between the shock wave and the turbulent boundary layer as well as between the external inviscid flow and the highly curved streamlines in the near wake at the trailing edge. Here we have to account for large normal pressure gradients, which cause the usual boundary layer assumptions to break down.

To properly describe the local interaction of a normal shock with the turbulent boundary layer we apply the analytical model of Bohning and Zierep [1,2], which yields non-asymptotic small perturbation solutions of the Navier-Stokes equations for a thin viscous sublayer adjacent to the wall and an inviscid shear layer for the main part of the boundary layer. These closed form solutions are embedded in an integral boundary layer method [3] and iteratively coupled via the displacement thickness concept to an outer potential flow solver in finite area formulation [4]. The wake is presently adjusted to the solution by pressure equality on its upper and lower surface.

Concerning the flow around a single airfoil the overall model we use, though different in its individual calculation procedures and their coupling, may be compared to the "Grumfoil"code by Melnik et al. [5], recently extended by Inger's shock-boundary layer interaction treatment [6]. While at present the "Grumfoil"algorithm takes better account of

* Research Scientist, Institute for Theoretical Fluid Mechanics, Member AIAA
Assistant Professor, Department of Aerospace Engineering and Engineering Mechanics, Member AIAA

strongly curved near wake flow, due to the implementation of the results of Melnik and Chow [7], our code incorporates a extra design option. As outlined already for inviscid cascade flow in [8] the fictitious gas concept is applied to provide surface modifications of the blade contour necessary to allow for shock-free flow at supercritical operating conditions. It's that flexibility of a code, which may be appreciated by the practising engineer, giving him a tool to analyse a given cascade's performance and redesign it in order to improve its efficiency.

Computational Grid Generation

Because of the periodic character of the cascade flow field we look for a geometrically periodic computational grid to enforce the periodicity conditions directly in the grid points without any interpolation. As transonic flow is very sensitve to small changes in blade contour, we want to apply the exact inviscid boundary conditions precisely at the effective airfoil surface which extends smoothly into the modeled wake via an open trailing edge. These requirements can be met by the use of a boundary conforming C-type grid which unwraps the high curvature region around the leading edge into a nearly planar surface in the computational domain.

Fortunately, using a finite area technique for the inviscid flow computation the grid does not have to possess strict orthogonality, which to obtain would be rather time consuming. Instead we can generate the mesh very economically by combining two analytically defined conformal mappings on to a strip of distorted rhomboidal cells followed by separate coordinate shearing and stretching transformations [9]. This will significantly speed up the overall procedure since the grid has to be repeatedly created for each global iteration cycle due to the varying displacement thickness.

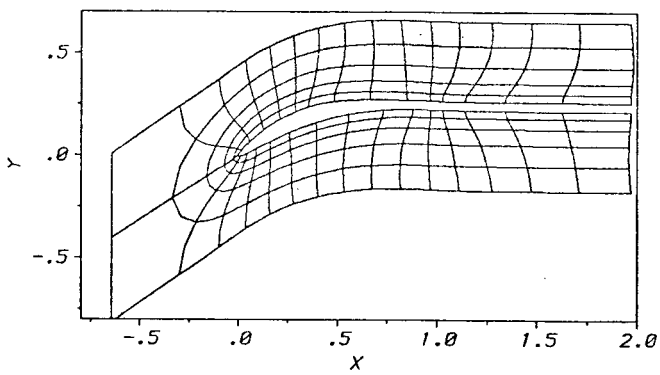

Fig. 1 C-Type Grid for a Staggered Compressor Cascade with Wake Included

A shockless flow field may be accurately resolved by a fixed bunching of body conforming grid lines near the airfoil surface and an a priori clustering of points around leading and near trailing edge. On the other hand, if there appear shocks varying in position during the iteration, the grid generation procedure should hold the possibility of clustering points while tracing the shock. The shock position can be predicted to no greater accuracy than the mesh spacing near it.

When a shock capturing technique is employed, the shock is approximated by strong gradients of the flow variables due to artificial viscosity added in the supersonic region. The distance over which the jump is smeared, is generally of the same order of magnitude as the shock-boundary layer interaction zone, especially at the high Reynolds numbers of interest. Thus the localization of the smearing yields another reason for smooth grid refinement at the shock. Since the artificial viscosity term scales with the mesh size, the coefficient of artifical viscosity may have to be increased locally corresponding to the extent to which the mesh spacing is reduced in order to keep numerical stability and avoid unphysical Mach number peaks just ahead of the shock.

Our grid generation procedure requires just the position along shock and the distance between two surface points where clustering additional to the leading and trailing edge regions is desired. A detail of the grid around a compressor blade shown in Fig. 1 is depicted in Fig. 2 : we see that the grid is clustered on the upper surface at x/c = 0.33.

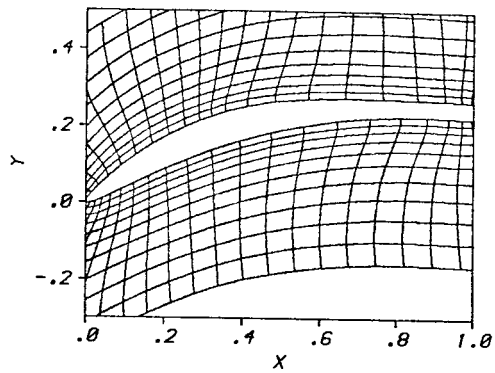

Fig. 2 Local Grid Clustering at x/c = 0; 0.33; 1

Inviscid Flow Analysis

As already mentioned we use the full potential equation (1)

$$\left(1-\frac{\phi_x^2}{a^2}\right)\phi_{xx}+2\frac{\phi_x\phi_y}{a^2}\phi_{xy}+\left(1-\frac{\phi_y^2}{a^2}\right)\phi_{yy}=0 \qquad (1)$$

to model the inviscid flow field. It may be regarded as the continuity equation for an isentropic flow of an ideal gas which we numerically solve in its divergence free form

$$(\rho u)_x+(\rho v)_y=0 \qquad (2)$$

to properly treat discontinuous solutions. Besides conservation of mass and energy we impose constant entropy as a third condition. Thus the momentum equation can't be satisfied also across shock waves, which means that the preshock Mach number should not be substantially greater than 1.3 to limit the deviations from the correct Rankine-Hugoniot jumps.

The different character of the potential equation in locally sub- and supersonic flow regions will be accounted for by type-dependent differencing. In a cartesian coordinate system, which is locally aligned with the streamline direction s, we approximate the second derivatives of ϕ by central differences (superscript E) and add artifical viscosity (superscript H) in grid points of supersonic flow corresponding to upstream differencing of ϕ_{ss}

$$(1-M^2)\phi_{ss}^E+\phi_{nn}^E+\xi_x^H+\eta_y^H=0$$

The finite area technique [4] used here to solve equation (2) actually represents finite differencing performed in a uniformly discretized rectangular computational plane. The computational grid is transformed from the physical plane (x,y) into the computational plane (X,Y). Employing the contravariant velocity vector component notation

$$\begin{Bmatrix} U \\ V \end{Bmatrix} = \begin{bmatrix} x_X & x_Y \\ y_X & y_Y \end{bmatrix} \begin{Bmatrix} u \\ v \end{Bmatrix}$$

the mass conservation equation becomes

$$\frac{1}{D}\left\{\left[(\rho DU)^E + \bar{\xi}^H\right]_X + \left[(\rho DV)^E + \bar{\eta}^H\right]_Y\right\} = 0$$

where D is the determinant of the transformation matrix. To solve the nonlinear difference equations generated by the discretization procedure this steady-state equation is embedded in an artificial time dependent equation.

The boundary condition on the airfoil then simply becomes

$$V = 0 .$$

Uniform flow conditions are enforced at the upstream and downstream flow field boundary.

Treatment of Viscous Layers

For the computation of the boundary layer we employ Rotta's integral dissipation method [3]. It solves simultaneously von Karman's momentum equation and the mechanical energy equation, utilizing additional empirical relations for the shape factors, the skin friction coefficient and the dissipation coefficient.

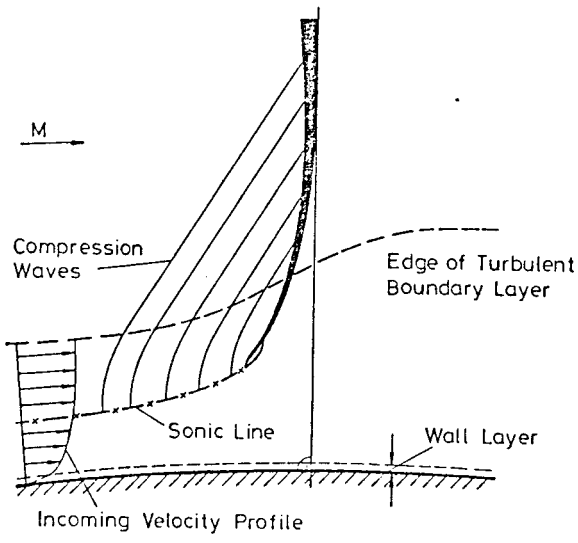

Fig. 3 Model of Shock Boundary Layer Interaction

When we march under the shock, normal pressure gradients cause a perturbation of the boundary layer. Neglecting the dependence of the undisturbed flow in streamwise direction within the small interaction region Bohning and Zierep derive linearized perturbation equations from the continuity, Navier-Stokes and energy equations. As their model has been already described in the literature [1,2] only a brief look at some of its essential features will be given here. Following Lighthill's concept the turbulent boundary layer is divided into two compressible layers. In the outer layer friction is only due to the incoming undisturbed velocity profile while the perturbations lend themselves to an essentially inviscid boundary value problem. Approximating the undisturbed velocity and Mach number profiles by power law functions the resulting second order differential equation is solved analytically containing the thickness of the inner wall layer as a yet unknown parameter. Whithin the inner layer, which turns out to be of the order of 1 % of the boundary layer thickness, the Mach number typically decreases from about 0.5 to zero at the wall. A closed form solution of linearized compressible boundary layer equations yields on one hand the thickness of this layer and on the other hand - in combination with a suitable law of the wall for the undisturbed profile - the wall shear stress.

As the basic incoming boundary layer quantities are frozen over the streamwise extent of the interaction region, the variations of the perturbations have to vanish at $x \to \pm\infty$. Thus the solution must exhibit an asymptotic behaviour. Actually, because of its exponential decay, the wall pressure perturbation e.g. tends to zero within a few boundary layer thicknesses (or say within 2% of chord typically). Having replaced the assumed analytical structure of the inviscid pressure distribution in the original version by the numerical calculation of the external flow field, we attach the perturbation solution to the ordinary boundary layer calculation at such streamwise locations that the latter will not be subjected to the sharp pressure rise across the shock. These locations, though depending on Reynolds number and grid refinement, are usually given by the extent of potential shock smearing due to artificial viscosity, as mentioned before. At the end of the interaction zone we have all possible integral boundary layer quantities at our disposal. Solving for the displacement thickness we evaluate δ_1 and the shape factor H_{32} at the end of the interaction and submit these quantities to reinitiate the boundary layer code.

Being based on a linearized perturbation analysis at M = 1 the interaction theory of Bohning and Zierep requires the preshock Mach number not to substantially exceed 1.3. Also, at greater Mach numbers separation may be likely to occur which can't be treated by the integral boundary layer method used. On the other hand comparison with experiment shows that the interaction theory may serve at least as a guide to incipient separation. Requiring numerical evaluation of closed from solutions only, the method of Bohning and Zierep takes but a small fraction of the whole computing time.

At present we treat the wake as a viscous displacement model of constant thickness given by the sum of the trailing edge and boundary layer displacement thicknesses. Instead of fulfilling the Kutta condition the wake is adjusted to the solution with regard to pressure equality on its upper and lower surfaces by iterating on its curvature only. Within the overall iteration process between inviscid and viscous parts of the flow field this concept can easily be extended to a more appropriate wake treatment including other parameters, e.g. variable wake displacement thickness and/or variable exit flow angle [10]. Furthermore, it holds the possibility of coupling the wake modeling with or partially substituting it by a viscous flow analysis at and behind the trailing edge. Figure 2 shows a rear loaded compressor blade with high trailing edge camber in order to provide a Stratford type pressure

distribution which, at least at operating conditions near design, should provide nonseparating boundary layers.

Viscid - Inviscid Coupling

In transonic flow over an airfoil we are concerned with regions of weak and strong viscid-inviscid interactions. The weak interaction arises from boundary layer displacement and global wake curvature effects. Here we have no convergence problems following the standard global iteration approach: we simply prescribe the inviscid pressure distribution as boundary condition for the boundary layer calculation and use as result the displacement thickness to correct the airfoil contour for viscous effects.

When adverse local pressure gradients cause stronger interaction the direct iteration approach becomes unstable. Damping of the instability is usually provided by underrelaxing the displacement thickness. At the very strong pressure gradients occuring due to shock waves or highly curved streamlines in the near wake this procedure would require vanishing relaxation coefficients, while at the same time the ordinary boundary layer equations are no longer adequate to describe the details of the physics.

Having partially accounted for this problem by employing the Bohning-Zierep interaction theory at the shock we still encounter stability problems at the trailing edge. At present we circumvent this shortcoming by linearly extrapolating the pressure distribution to be submitted to the boundary layer code at about 97% chord up to the trailing edge.

In the potential flow calculation we use a fourfold grid sequence, each time halving the mesh width. In order to save time we could use the ordinary boundary layer integral code on a coarse grid during the first iterations even in the shock region, if the pressure gradient would be sufficiently smeared. Hence we introduce a simple analytical function to widely smear out the pressure rise across the inviscid shock for the first two iterations. In fact the adverse velocity gradients predicted by purely inviscid theory in regions of strong interaction are much greater (theoretically infinite) than they will be in the final converged state. So all we do is to anticipate qualitatively a part of the later result and at the same time exaggerate it in a certain sense. Thus the boundary layer code doesn't signalize separation during the early stage of the iterative process. In order to get a smooth transition to the actually calculated inviscid pressure distribution, which is submitted to the viscous part of the employed local analysis on the third and fourth grid, we also underrelax the pressure. Applying this simple procedure the shock hardly moves and convergence is generally obtained after 5 to 7 cycles.

Having outlined the simple viscous/inviscid coupling procedure we renounce presenting the usual block diagram of the overall computation process and pursue instead the development of the solution by means of an illustrative example calculation.

Results

In order to minimize effects of the trailing edge, where our treatment of the viscous flow still needs substantial improvements, we choose as a first example the symmetrical NACA 0012 profile at zero incidence and a free stream Mach Number of 0.77. Starting the iterative cycle on a coarse grid with only 20 mesh points along the upper surface of the bare profile the resulting pressure distribution of the inviscid flow field calculation shown in Fig. 4 a is analytically smeared out over the shock region. Thus the ordinary boundary layer method employed over the whole profile up to the third iteration does not immediately signalize turbulent separation. The resulting displacement thickness (indicated by crosses in Fig. 4 a) is underrelaxed (solid line in Fig. 4 b) before it is added to the profile contour. At the 3rd and 4th steps (Fig. 4 c, d) the grid size is halved each time. On these finer meshes the calculation of the inviscid flow over the smoothly curved convex effective profile develops the singular behaviour of the pressure at the shock root. Henceforth on the finest grid (Fig. 4 d, e,f,g) the interaction theory is employed in the shock region and the whole viscous calculation subjected to an underrelaxed pressure distribution. The main effect of also relaxing the pressure is again to smear out the jump while the shock is still moving during the iteration and thus to stabilize the process of finding stationary positions of the shock and the accompanying boundary layer thickening. Finally, when convergence is achieved, the boundary layer is subjected to the correct pressure distribution, its jump across the shock being felt as sharp as provided by the inviscid flow field calculation in connection with local grid clustering. Since our finite area code can handle the bumps in displacement thickness produced by the interaction theory no additional smoothing is needed. Thus the very small change in displacement thickness occuring at transition from laminar to turbulent boundary laye (x/c = 0,07) becomes evident in a small flaw in the pressure distribution (Fig. 4 g).

When the inviscid flow begins to react with the sudden increase in displacement thickness (Fig. 4 e, f,g) the before singular behaviour of the pressure at the shock root gradually vanishes. The resulting local distribution resembles one that would appear when the boundary layer thickening had been modeled as a viscous ramp [11,12]. Consequently the shock approaching the profile surface bends towards upstream and becomes oblique, the deflection angle lying roughly within the limits given for sonic conditions and an attached shock respectively. This feature is also confirmed by experimental observations. For the pre- and postshock Mach numbers taken from the NACA 0012 example calculation the shock polar diagram Fig. 5 leads to a deflection angle of 3.85°. While the weak solution is observed for a postshock accelerating flow [12], we encounter the strong solution (left of point P in Fig. 5) for continuously decelerating flow.

Changing over to a typical user oriented problem we analyse as another illustrative example a supercritical blade section developed and tested by Rechter et al. [13] for a transonic compressor stator at an inlet Mach number of 0.8. The design aims at a shockfree recompression with attached boundary layer and acceptably low losses in the near off-design range. Fig. 6 shows the prescribed design Mach number distribution as a solid line together with some measured values from experimental verification. On the suction side flow deceleration starts rapidly and becomes more gradual at about 60 % of the chord length. While the discrepancies at the leading edge are due to limitations of

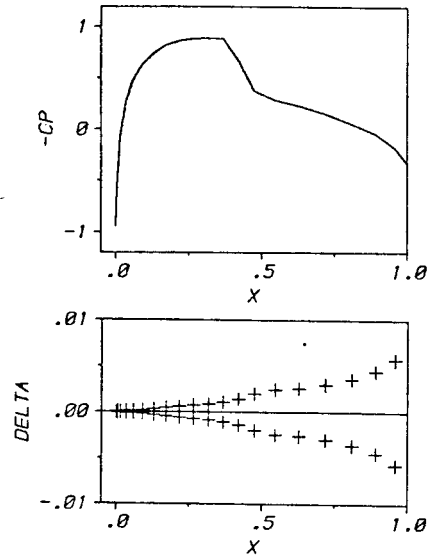

a) $\omega = 0.5$

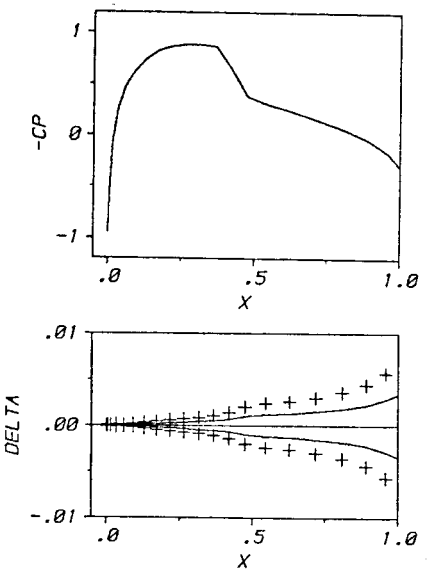

b) $\omega = 0.5$

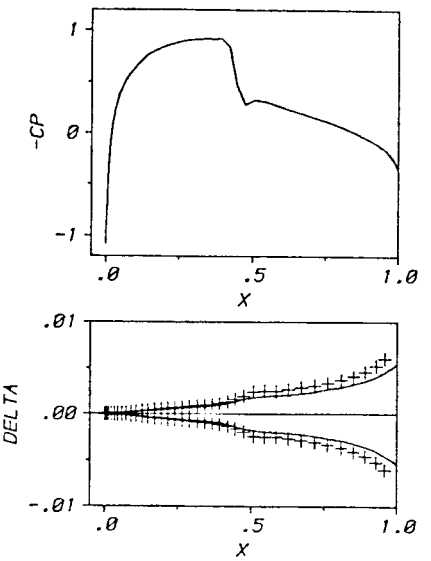

c) $\omega = 0.6$

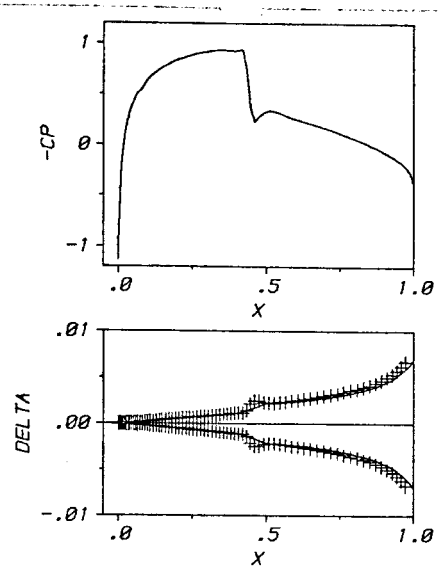

d) $\omega = 0.7$
shock boundary layer interaction

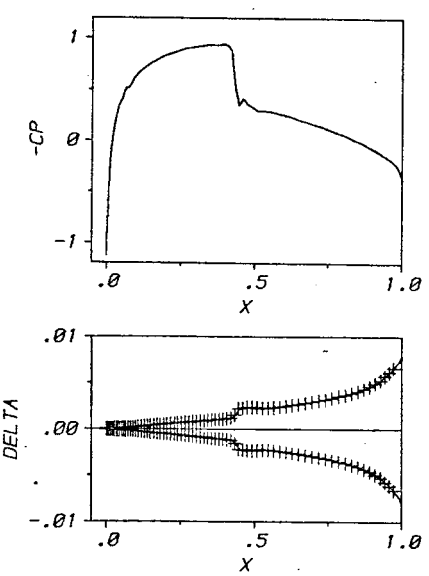

e) $\omega = 0.8$
shock boundary layer interaction

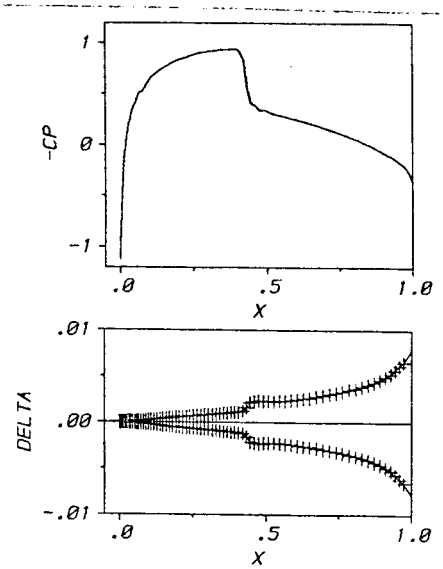

f) $\omega = 0.9$
shock boundary layer interaction

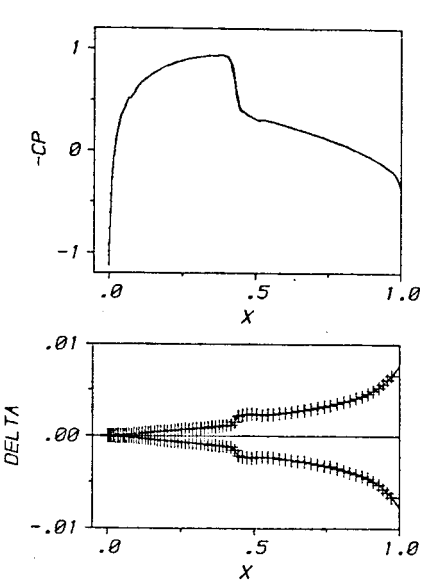

g) $\omega = 1.0$
shock boundary layer interaction

Fig. 4 Interative Sequence of Pressure Coefficient and Displacement Thickness for NACA 0012 Profile
($M_\infty = 0.77$; $Re = 4.9 \cdot 10^6$; $\alpha = 0°$)

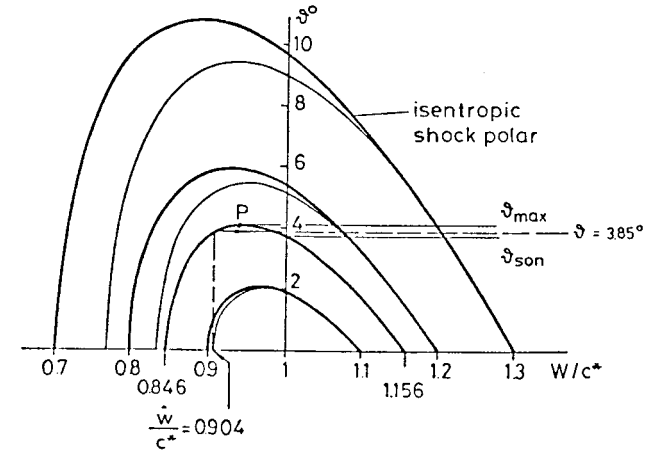

Fig. 5 Deflection Angle Across Shock

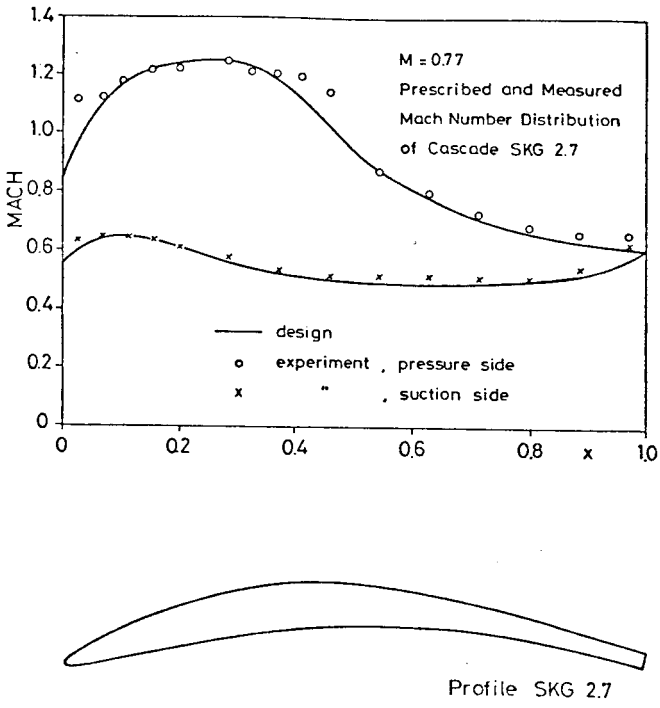

Fig. 6 Preseribed and Measured Mach Number Variation for the SKG 2.7 Cascade (Ref. [13])

Schmidt's design method [14] the disagreement at about 40% of chord length was attributed to a laminar separation bubble.

Our analysis is based on the profile data given except for the leading edge region, which was rather coarsely displayed and needed some modifications. Letting transition take place near laminar separation we encountered shock induced transition. As the treatment of shock-transitional boundary layer interaction is beyond the capabilities of our code we speficified with reference to [13] transition at 30% of the chord length. This time a fairly strong shock impinges on a turbulent boundary layer at x = 0.36 (Fig. 7) and a further modest increase in inflow Mach number from 0.8 to 0.81 instantaneously caused turbulent boundary layer separation.

It would certainly be unsatisfactory for the practising engineer to stop at this stage of analysis. Fortunately we can switch over to the design option of the code and slightly modify the profile section on the suction surface in order to provide shock free flow at operating conditions [8]. Fig. 8 shows the pressure distribution partially obtained by the method of characteristics for the redesigned blade section. Subsequent analysis of the inviscid flow through the redesigned cascade with displacement thickness added to the profile reveals an indentation in the pressure distribution (Fig. 9).

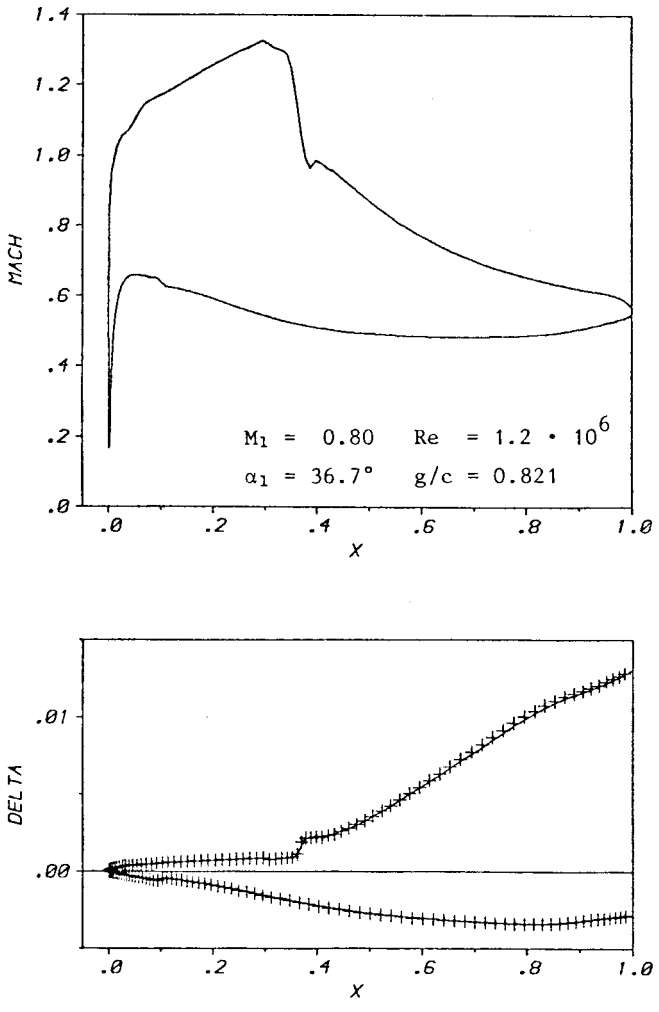

Fig. 7 Analysis of SKG 2.7 Cascade

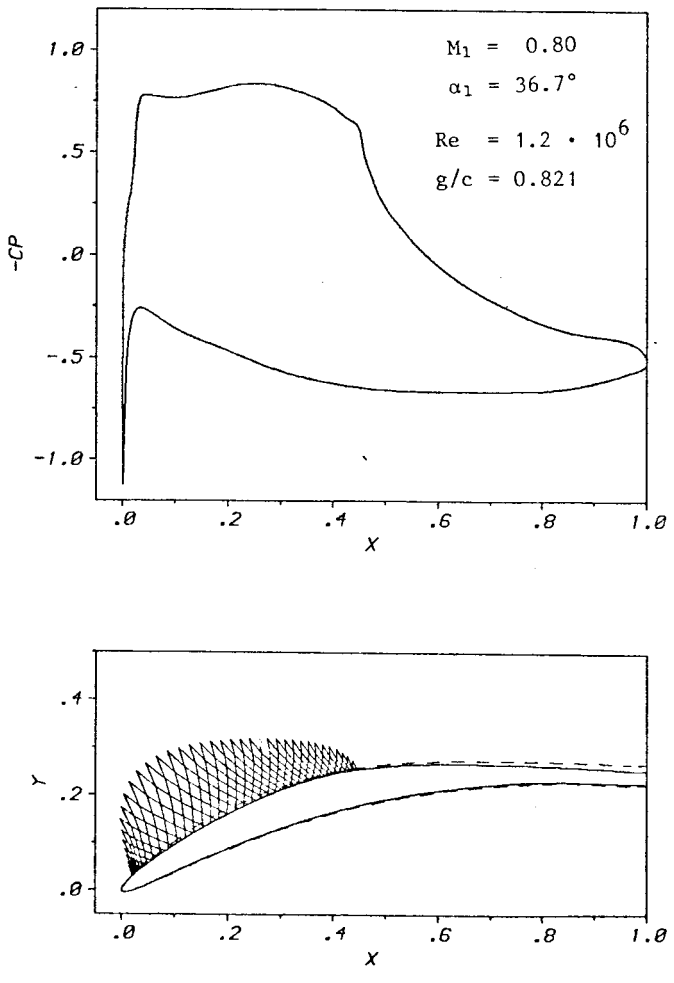

Fig. 8 Prescribed Pressure Distribution for Redesigned Cascade

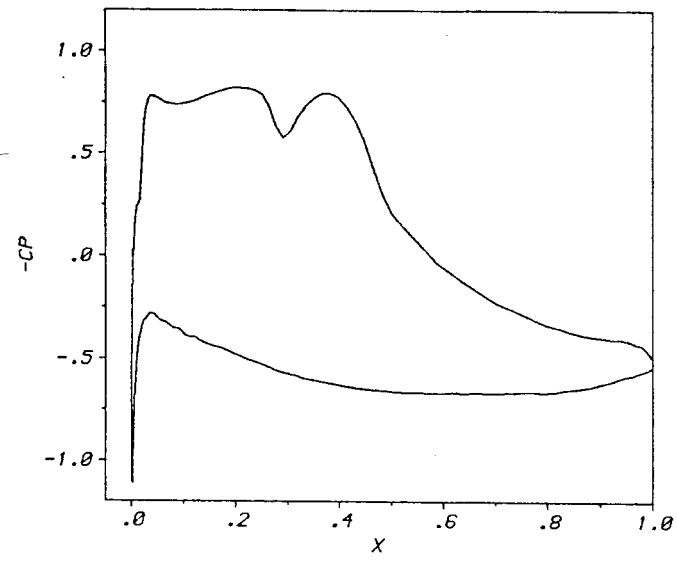

Fig. 9 Analysis of outer Inviscid Flow around Redesigned Cascade Including Displacement Thickness

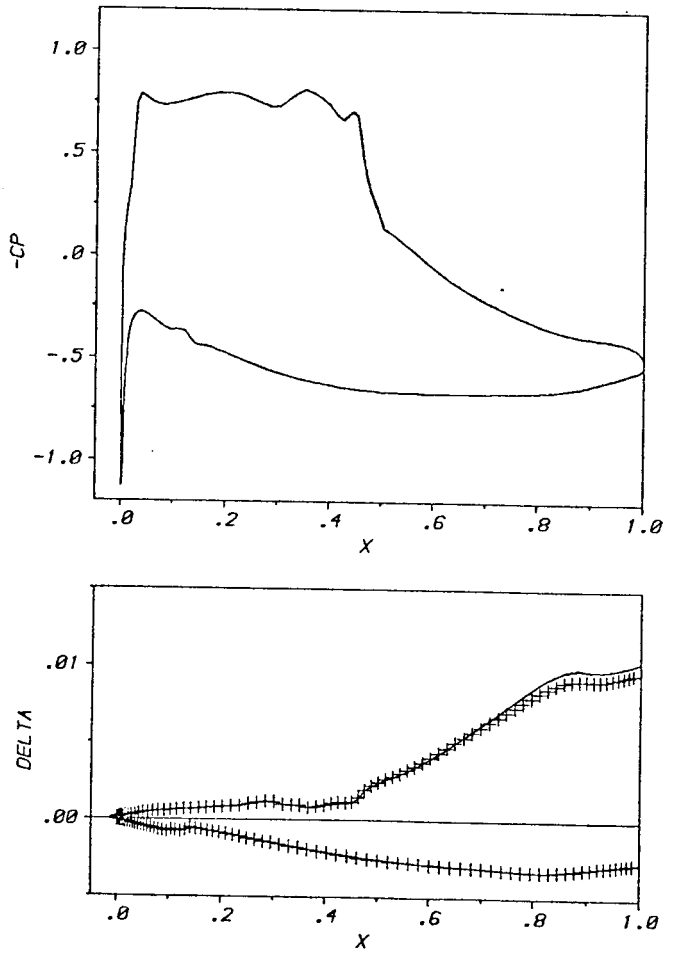

g. 10 Complete Analysis of Redesigned Cascade
a. Variation of Pressure Coefficient
b. Variation of Displacement Thickness

Having subtracted the displacement thickness we again analyse the complete inviscid/viscous flow field starting from the bare profile and recovering a nearly shock free solution (Fig. 10). The preshock wiggles appearing in the pressure distribution may possibly originate from the aforeshown indentation (Fig. 9) interacting with the supersonic part of the boundary layer in the course of the iteratively developing solution. From Figs. 8 to 10 it becomes evident that there is some latitude between prescribed design values and the results obtained from numerical analysis due to different accuracies of the various methods employed and to the high sensivity of transonic flow to small changes in the effective contour. Slightly raising the inflow Mach number from 0.8 to 0.81 (Fig. 11) causes increasing shock losses, but the severe limit of this tough test case is given by turbulent boundary layer separation, which occurs just beyond M = 0.81.

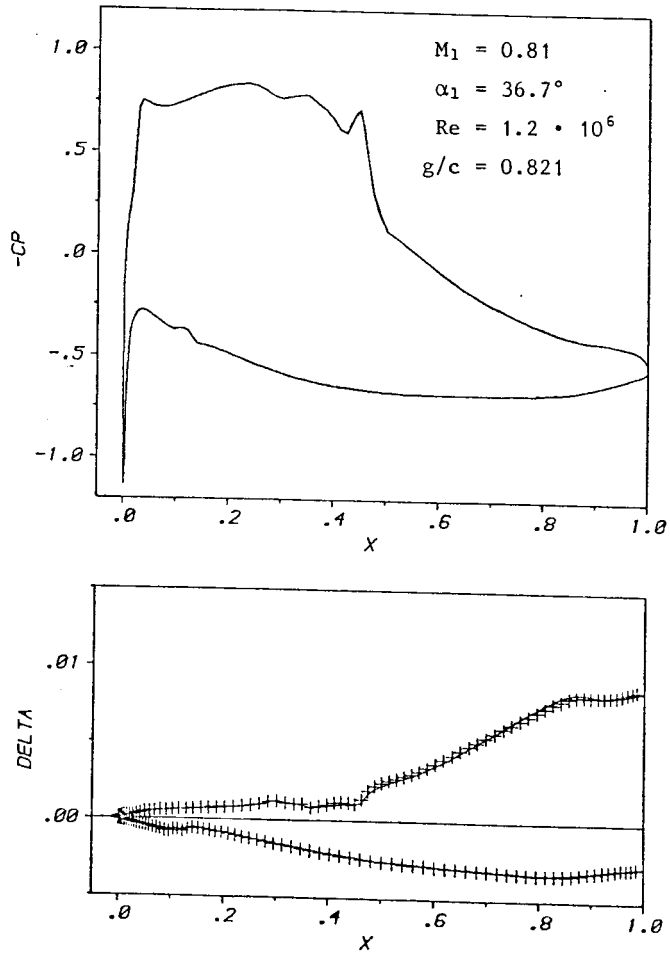

Fig. 11 Off-Design Analysis of Redesigned Cascade
a. Variation of Pressure Coefficient
b. Variation of Displacement Thickness

Conclusion

We have described the extension of an efficient numerical analysis and design tool for engineering purposes to take into account shock boundary layer interaction at cascades' off-design performance. An easy mapping procedure, a smooth local grid clustering, an analytical solution for the viscous interaction zone, a simple direct coupling and iterative solution technique are the main features of the modules contributing to that extension. The flexible applicability of the code has been demonstrated by a user oriented example calculation. Consideration of quasi 3-dimensional effects and a more adequate wake modeling belong to further improvements being under development.

References

1. Bohning, R., Zierep, J., Der senkrechte Verdichtungsstoß an der gekrümmten Wand, ZAMP, Vol. 27, 1976, pp. 225-240

2. Bohning, R., Zierep, J., Normal shock - turbulent boundary layer interaction at a curved wall, AGARD CP-291, 1980, pp. 17/1 - 17/8

3. Rotta, J.C., Turbulent boundary layer calculations with the integral dissipation method, Computation of Turbulent Boundary Layers - 1968 AFOSR - IFP Stanford Conference, Vol. I, p. 177 (also Ing. Archiv, Vol. 38, 1969, pp. 212-222)

4. Dulikravich, D.S., Sobieczky, H., Shockless design and analysis of transonic cascade shapes, AIAA Journal, Vol. 20, Nr. 11, 1982, pp. 1572-1578

5. Melnik, R.E., Chow, R., Mead, H.R., Theory of viscous transonic flow over airfoils at high Reynolds number, AIAA - Paper, 77-680, 1977

6. Lekoudis, S.G., Inger, G.R., Computation of the viscous transonic flow around airfoils with trailing edge effects and proper treatment of the shock/boundary layer interaction, AIAA - Paper, 82-0989, 1982

7. Melnik, R.E., Chow, R., Asymptotic theory of two-dimensional trailing edge flows, NASA SP 317, 1975

8. Sobieczky, H., Dulikravich, D.S., A computational design method for transonic turbomachinery cascades, ASME - Paper, 82-GT-117, 1982

9. Dulikravich, D.S., Fast grid generation of threedimensional computational boundary - conforming periodic grids of C-type, NASA/AFOSR - Symposium on Numerical Generation of Curvilinear Coordinate Systems and use in the Numerical Solution of Partial Differential Equations, Nashville, April 13-16, 1982

10. Hobbs, D.E., Wagner, J.H., Dannenhoffer, J.F., Dring, R.P., Experimental investigation of compressor cascade wakes, ASME - Paper, 82-GT-299, 1982

11. Sobieczky, H., The design of transonic airfoils under consideration of shock wave boundary layer interaction, DFVLR-Report IB 251-76 A 26, 1976

12. Jou, W.H., Murmann, E.M., A phenomenological model for displacement thickness effects of transonic shock wave-boundary layer interactions, AGARD-CP-291, 1981, 15/1 - 15/9

13. Rechter, H., Schimming, P., Starken, H., Design and testing of two supercritical compressor cascades, ASME - Paper, 79-GT-11, 1979

14. Schmidt, E., Computation of supercritical compressor and turbine cascades with a design method for transonic flows, ASME - Paper, 79-GT-30, 1979